Seventh South African Conference on Computational and Applied Mechanics
SACAM10
Pretoria, 10−13 January 2010

ACCURACY OF SEMI-ANALYTICAL FINITE ELEMENTS FOR MODELLING WAVE PROPAGATION IN RAILS

Eshwar V. Andhavarapu[⋆†,1], Philip Loveday[⋆,2], Craig S. Long[⋆,3] and P. Stephan Heyns[†,4]

[⋆]Sensor Science & Technology, CSIR Material Science and Manufacturing,
P O Box 395, Pretoria 0001, South Africa,
[1]EAndhavarapu@csir.co.za,[2]PLoveday@csir.co.za,[3]CLong@csir.co.za
[†]Dynamic Systems Group, Department of Mechanical and Aeronautical Engineering,
University of Pretoria, Pretoria, South Africa,
[4]Stephan.Heyns@up.ac.za

Keywords: Guided Waves, Semi-Analytical Finite Element Method, Rail

Abstract

The semi-analytical finite element method (SAFE) is a popular method for analysing guided wave propagation in elastic waveguides of complex cross-section such as rails. The convergence of these models has previously been studied for linear triangular elements. This paper extends this study to include quadratic triangular elements and other linear and quadratic elements. It is shown that for a given number of degrees of freedom the quadratic elements are more efficient than the linear elements. Based on the results of the convergence studies presented here, the use of quadratic quadrilateral elements is recommended and these may be complemented by quadratic triangular elements if necessary. The use of symmetry and anti-symmetry boundary conditions when modelling rails was also investigated. It was found that these models predict all the modes of propagation within the frequencies investigated. The use of this approach is therefore recommended for elastic waveguides with symmetrical cross-section.

1 Introduction and Objectives

The semi-analytical finite element method (SAFE) is becoming popular for analysing guided wave propagation in elastic waveguides of complex cross-section such as rails [1, 2, 3, 4]. The method has been combined with conventional three dimensional finite element models of piezoelectric ultrasonic transducers to predict the transducer performance [5]. These transducers operate at frequencies where a large number of waves propagate in the rail and accurate modelling of the excitation of the waves requires accurate modelling of the rail characteristics. A convergence study was presented in [2] but this study considered only linear triangular elements. In this paper we extend the study to consider linear and quadratic triangular and quadrilateral elements. The first objective is to determine which of the elements is most efficient for modelling a rail in the high frequency range. Recently the SAFE has been applied to model a rail using only half the cross-section of the rail and symmetry and anti-symmetry boundary conditions [6]. Apart from reducing the size of the problem this method may make it easier to separate the different modes of propagation. The modes of propagation predicted

by this model are either symmetric or anti-symmetric, depending on the boundary conditions applied. The question of practical interest is whether any important modes (for guided wave ultrasound applications) are absent or inaccurately predicted when this approach is followed. The second objective of this paper is to answer this question.

2 Semi-Analytical Finite Element Formulation

In the SAFE, as described in [7], the displacement field in an elastic waveguide, extending in the z direction, is described by a complex exponential along the waveguide and a finite element approximation over the cross-section. The displacement fields (u, v, w) can be written as:

$$\begin{aligned} u(x,y,z,t) &= u(x,y).e^{-j(\kappa z-\omega t)} \\ v(x,y,z,t) &= v(x,y).e^{-j(\kappa z-\omega t)} \\ w(x,y,z,t) &= j.w(x,y).e^{-j(\kappa z-\omega t)} \end{aligned} \tag{1}$$

where z is the coordinate in the direction along the waveguide, κ the wavenumber and ω the frequency.

The strains are also written as a function of the strains over the cross-section multiplied by a complex exponential as follows:

$$\epsilon(x,y,z,t) = \epsilon(x,y).e^{-j(\kappa z-\omega t)} \tag{2}$$

The definition of strain energy of an infinitesimal element of the waveguide is:

$$S.E. = \frac{1}{2}\epsilon^*.c.\epsilon = \frac{1}{2}[\kappa^2.k_2 + \kappa.k_1 + k_0] \tag{3}$$

where $*$ denotes the complex transpose. k_0, k_1 and k_2 – the element stiffness matrices – are defined below; ϵ and c are the strain vector and elasticity matrix that are defined as follows:

$$\epsilon(x,y,z,t) = \left\{ \begin{array}{c} \frac{\partial u}{\partial x} \\ \frac{\partial v}{\partial y} \\ \frac{\partial w}{\partial z} \\ \frac{\partial u}{\partial y} + \frac{\partial v}{\partial x} \\ \frac{\partial v}{\partial z} + \frac{\partial w}{\partial y} \\ \frac{\partial u}{\partial z} + \frac{\partial w}{\partial x} \end{array} \right\} \tag{4}$$

$$c = \frac{E}{(1+\nu)(1-2\nu)} \begin{bmatrix} 1-\nu & \nu & \nu & \cdot & \cdot & \cdot \\ \nu & 1-\nu & \nu & \cdot & \cdot & \cdot \\ \nu & \nu & 1-\nu & \cdot & \cdot & \cdot \\ \cdot & \cdot & \cdot & \frac{1-2\nu}{2} & \cdot & \cdot \\ \cdot & \cdot & \cdot & \cdot & \frac{1-2\nu}{2} & \cdot \\ \cdot & \cdot & \cdot & \cdot & \cdot & \frac{1-2\nu}{2} \end{bmatrix} \tag{5}$$

where E is Young's Modulus and ν is Poisson's ratio.

For convenience in further development, terms that are dependent on the wavenumber, κ are separated from the independent terms as:

$$\epsilon(x,y) = \epsilon_0(x,y) + \kappa\epsilon_1(x,y) \tag{6}$$

$$\epsilon_0(x,y) = \begin{Bmatrix} \frac{\partial u(x,y)}{\partial x} \\ \frac{\partial v(x,y)}{\partial y} \\ 0 \\ \frac{\partial u(x,y)}{\partial y} + \frac{\partial v(x,y)}{\partial x} \\ \frac{\partial w(x,y)}{\partial y} \\ \frac{\partial w(x,y)}{\partial x} \end{Bmatrix} \tag{7}$$

$$\epsilon_1(x,y) = \frac{1}{\kappa}\begin{Bmatrix} 0 \\ 0 \\ \frac{\partial w}{\partial z} \\ 0 \\ \frac{\partial v}{\partial z} \\ \frac{\partial u}{\partial z} \end{Bmatrix} = \frac{1}{\kappa}\begin{Bmatrix} 0 \\ 0 \\ \kappa w(x,y) \\ 0 \\ -j\kappa v(x,y) \\ -j\kappa u(x,y) \end{Bmatrix} = \begin{Bmatrix} 0 \\ 0 \\ w(x,y) \\ 0 \\ -jv(x,y) \\ -ju(x,y) \end{Bmatrix} \tag{8}$$

The terms in the strain energy can now be expressed as follows:

$$\begin{gathered} k_0 = \epsilon_0^* c \epsilon_0 \\ k_1 = \epsilon_0^* c \epsilon_1 + \epsilon_1^* c \epsilon_0 \\ k_2 = \epsilon_1^* c \epsilon_1 \end{gathered} \tag{9}$$

In the case of free vibration, applying finite element discretization over the cross-section produces the system equations of motion for the waveguide as follows (see [1, 5] for details):

$$M\ddot{U} + [\kappa^2.K_2 + \kappa.K_1 + K_0]U = 0 \tag{10}$$

where M denotes the global mass matrix and K_i denote global stiffness matrices.

3 Element Implementation

The iso-parametric formulation [8] was used to implement the SAFE described above. The interpolation matrix N relates the nodal degrees of freedom to the co-ordinates and displacement distributions as follows:

$$\begin{gathered} f(\xi,\eta) = \sum_{i=1}^{n} N_i(\xi,\eta) f_i \\ f = \begin{bmatrix} a_1 & b_1 & c_1 & a_2 & b_2 & c_2 & \dots & a_n & b_n & c_n \end{bmatrix}^T \end{gathered} \tag{11}$$

where (a, b, c) can either represent the nodal co-ordinates (x, y, z) or the nodal displacements (u, v, w). n represents the number of nodes per element. For this paper, 5 elements were used in the evaluation; the linear elements — Q4 & T3 — and quadratic elements — Q8, Q9 & T6 — where Q denotes quadrilateral elements and T denotes triangular elements.

The strain terms can be defined in terms of the local co-ordinates (ξ, η) by using (11) above. The Jacobian matrix for the co-ordinate transformation between the (ξ, η) space and the (x, y) space is given as follows:

$$J = \begin{bmatrix} J_{11} & J_{12} \\ J_{21} & J_{22} \end{bmatrix} = \begin{bmatrix} \frac{\partial x}{\partial \xi} & \frac{\partial y}{\partial \xi} \\ \frac{\partial x}{\partial \eta} & \frac{\partial y}{\partial \eta} \end{bmatrix} \tag{12}$$

The strain terms in local co-ordinates are then given by:

$$\begin{aligned} \epsilon_0(\xi,\eta) &= B_0(\xi,\eta)q \\ \epsilon_1(\xi,\eta) &= B_1(\xi,\eta)q \\ q &= \begin{bmatrix} u_1 & v_1 & w_1 & u_2 & v_2 & w_2 & \dots & u_n & v_n & w_n \end{bmatrix}^T \end{aligned} \tag{13}$$

where q is the nodal displacement vector and B_0 and B_1 are defined such that:

$$\begin{aligned} k_0 &= \int B_0^* c B_0 \left|J\right| \partial\xi\partial\eta \\ k_1 &= \int \left[B_0^* c B_1 + B_1^* c B_0\right] \left|J\right| \partial\xi\partial\eta \\ k_2 &= \int B_1^* c B_1 \left|J\right| \partial\xi\partial\eta \\ m &= \int N^* \rho N \left|J\right| \partial\xi\partial\eta \end{aligned} \tag{14}$$

This results in the strain terms being defined as follows:

$$\epsilon_0(x,y) = \begin{Bmatrix} \frac{\partial u(x,y)}{\partial x} \\ \frac{\partial v(x,y)}{\partial y} \\ 0 \\ \frac{\partial u(x,y)}{\partial y} + \frac{\partial v(x,y)}{\partial x} \\ \frac{\partial w(x,y)}{\partial y} \\ \frac{\partial w(x,y)}{\partial x} \end{Bmatrix}$$

$$= \frac{1}{|J|} \begin{bmatrix} J_{22} & -J_{12} & \cdot & \cdot & \cdot & \cdot \\ \cdot & \cdot & -J_{21} & J_{11} & \cdot & \cdot \\ \cdot & \cdot & \cdot & \cdot & \cdot & \cdot \\ -J_{21} & J_{11} & J_{22} & -J_{12} & \cdot & \cdot \\ \cdot & \cdot & \cdot & \cdot & -jJ_{21} & -jJ_{11} \\ \cdot & \cdot & \cdot & \cdot & jJ_{22} & -jJ_{12} \end{bmatrix} \begin{bmatrix} \frac{\partial u(\xi,\eta)}{\partial \xi} \\ \frac{\partial u(\xi,\eta)}{\partial \eta} \\ \frac{\partial v(\xi,\eta)}{\partial \xi} \\ \frac{\partial v(\xi,\eta)}{\partial \eta} \\ \frac{\partial w(\xi,\eta)}{\partial \xi} \\ \frac{\partial w(\xi,\eta)}{\partial \eta} \end{bmatrix} \tag{15}$$

$$\epsilon_1(x,y) = \begin{Bmatrix} 0 \\ 0 \\ w(x,y) \\ 0 \\ -jv(x,y) \\ -ju(x,y) \end{Bmatrix} = \begin{bmatrix} \cdot & \cdot & \cdot \\ \cdot & \cdot & \cdot \\ \cdot & \cdot & 1 \\ \cdot & \cdot & \cdot \\ \cdot & -j & \cdot \\ -j & \cdot & \cdot \end{bmatrix} \begin{Bmatrix} u \\ v \\ w \end{Bmatrix} \tag{16}$$

The integrals in (14) were evaluated at element level using Gauss-quadrature based numerical integration techniques as described in [8]. The global matrices – K and M – were sparse. To ensure full integration, 9 points were used in the case of quadrilateral elements and 6 in the case of triangular elements. Values for κ were selected and the eigenvalues for the problem in (10) were calculated using a sparse eigenvalue solver.

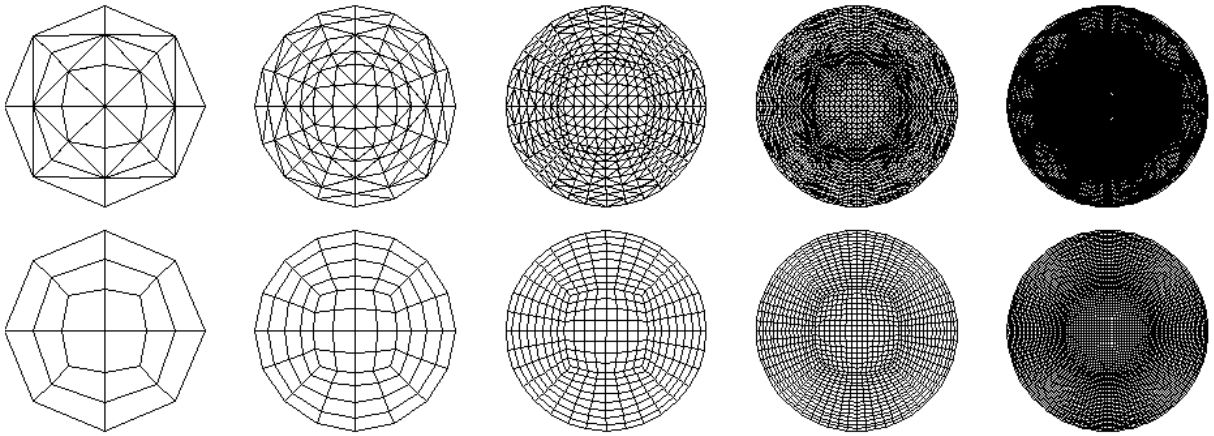

Figure 1: Element meshes for solid circular cylinder — triangular elements (top) and quadrilateral elements (bottom)

4 Numerical Results

In this section, numerical results of a convergence study, performed on a cylindrical waveguide are presented for the five element types selected for evaluation. A convergence study on a rail is also presented. Finally, the use of symmetric and anti-symmetric boundary conditions is investigated for the symmetrical rail profile.

4.1 Wave Propagation in a Solid Cylindrical Waveguide

The convergence study performed in [2] considered only linear triangular elements. The study is repeated here to verify the integrity of the SAFE implementation, as well as to evaluate the proposed linear and quadratic elements. To compare with the results obtained in [2] the dimension-less frequency, $\Omega = \omega a/c_{shear}$ was calculated, where ω is the frequency (rad/s), a is the radius of the cylinder (m) and c_{shear} is the sound velocity in shear (m/s) given by $\sqrt{G/\rho}$ where G is the shear modulus (Pa) and ρ is the material density (kg/m^3). The variables used to determine the rate of convergence were also the same as those used in [2] viz. the natural logarithm of the absolute error in the cut-off frequency vs. the natural logarithm of the square root of the number of elements.

A circular cylinder of radius, $a = 1m$ and $\nu = 0.3$ was modelled for this problem and the subsequent convergence study. The meshes in Figure 1 were used for the analysis. Each successive mesh was created so that it had 4 times the number of elements of the previous mesh.

The analytical values that were presented in [2] were first verified using [9]. These values were then used to reproduce Figure 2, which shows the convergence for the linear triangular elements and is equivalent to the results presented in [2]. The points in Figure 2 represent the calculated values and the lines represent the least square fit used to calculate the convergence. The result obtained here verifies the implementation of the SAFE method and allows us to proceed to compare the various elements. The parameters used for the convergence study in [2], especially the $\ln\sqrt{N_{el}}$ parameter, would favour the higher order elements and therefore new parameters were selected for the convergence study. To this end, the results from various elements were plotted and compared using the number of degrees of freedom instead of the

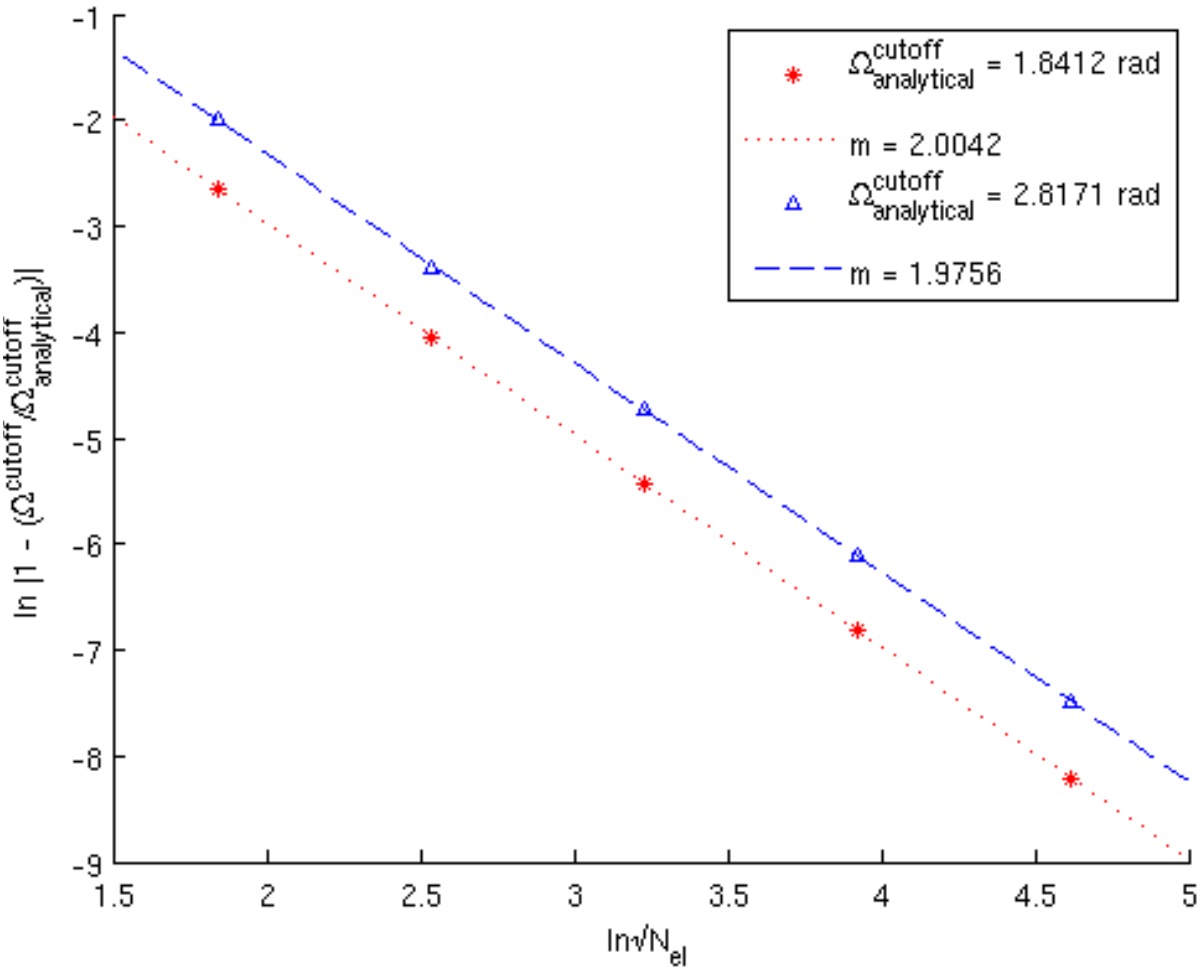

Figure 2: Convergence rates for selected cut-off frequencies

number of elements.

Figure 3 shows that — as in the traditional finite element implementation — the quadratic elements are more accurate than the linear elements for the same number of degrees of freedom. In the bottom half of Figure 3, the focus is on the quadratic elements which clearly shows that of the quadratic elements, the Q8 provides accuracy very similar to that of the Q9 or T6 but requires fewer degrees of freedom.

Figure 4 shows the same modes as shown in Figure 3 with the vertical axis now showing the percentage difference from the best value obtained for the Q8 element. It is again clear that the quadratic elements are much more accurate than the linear elements. It is also seen that the Q9 and T6 elements provide similar accuracy as the Q8 elements but for more degrees of freedom.

Based on these observations, the frequencies calculated for the finest mesh of Q8 elements were used as a reference value to calculate the absolute error as a fraction of the reference value. The finest meshes for the Q9 and T6 meshes were also omitted from the convergence study as the values obtained were very similar to the Q8 values, and could therefore compromise the convergence rates calculated.

Figure 5 once again shows that the quadratic elements converge much faster than the linear

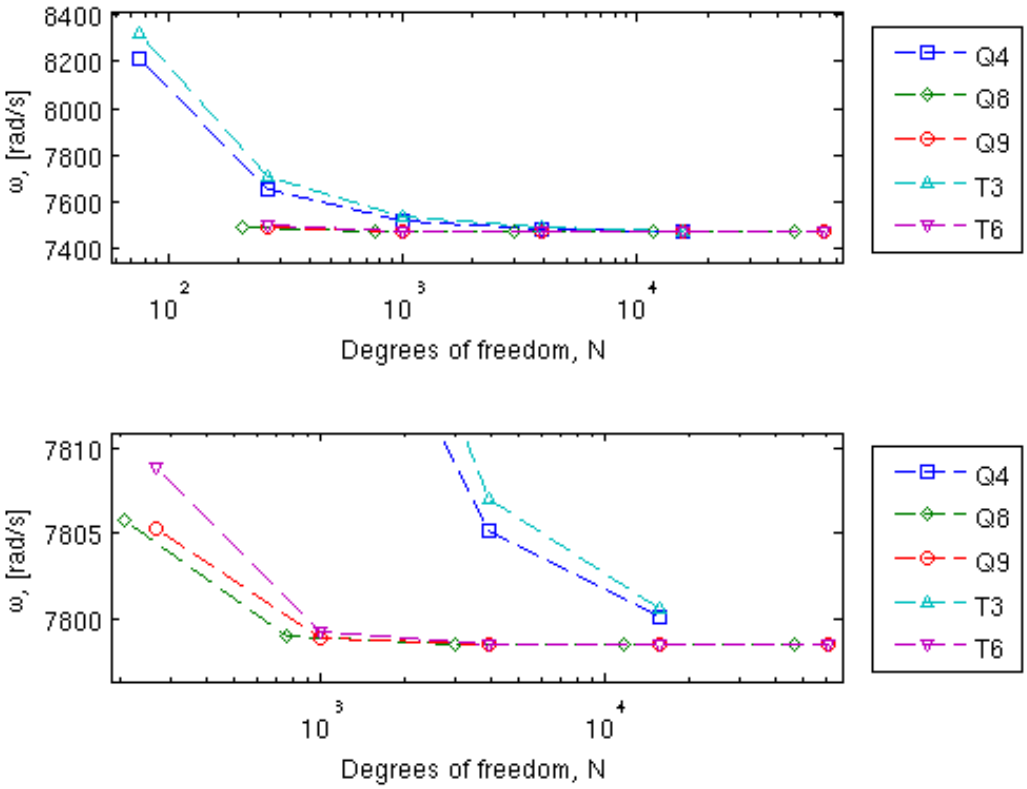

Figure 3: Convergence of two different modes with increasing degrees of freedom in the circular cylinder

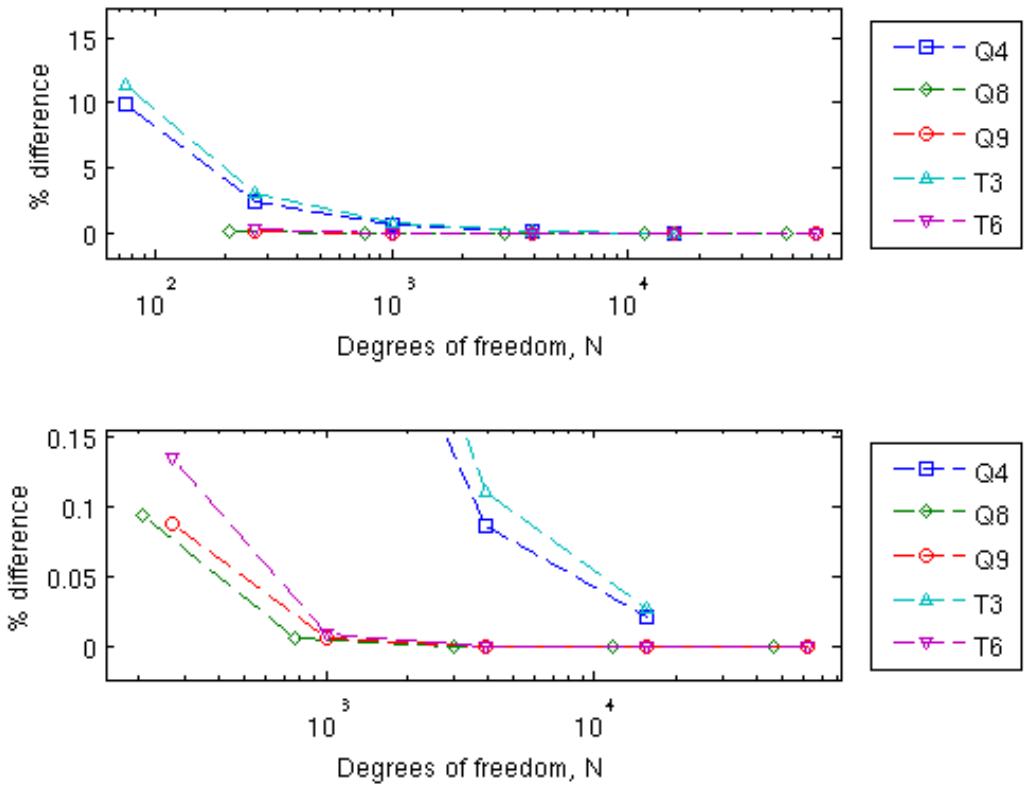

Figure 4: Percentage difference with the best value obtained for the Q8 element

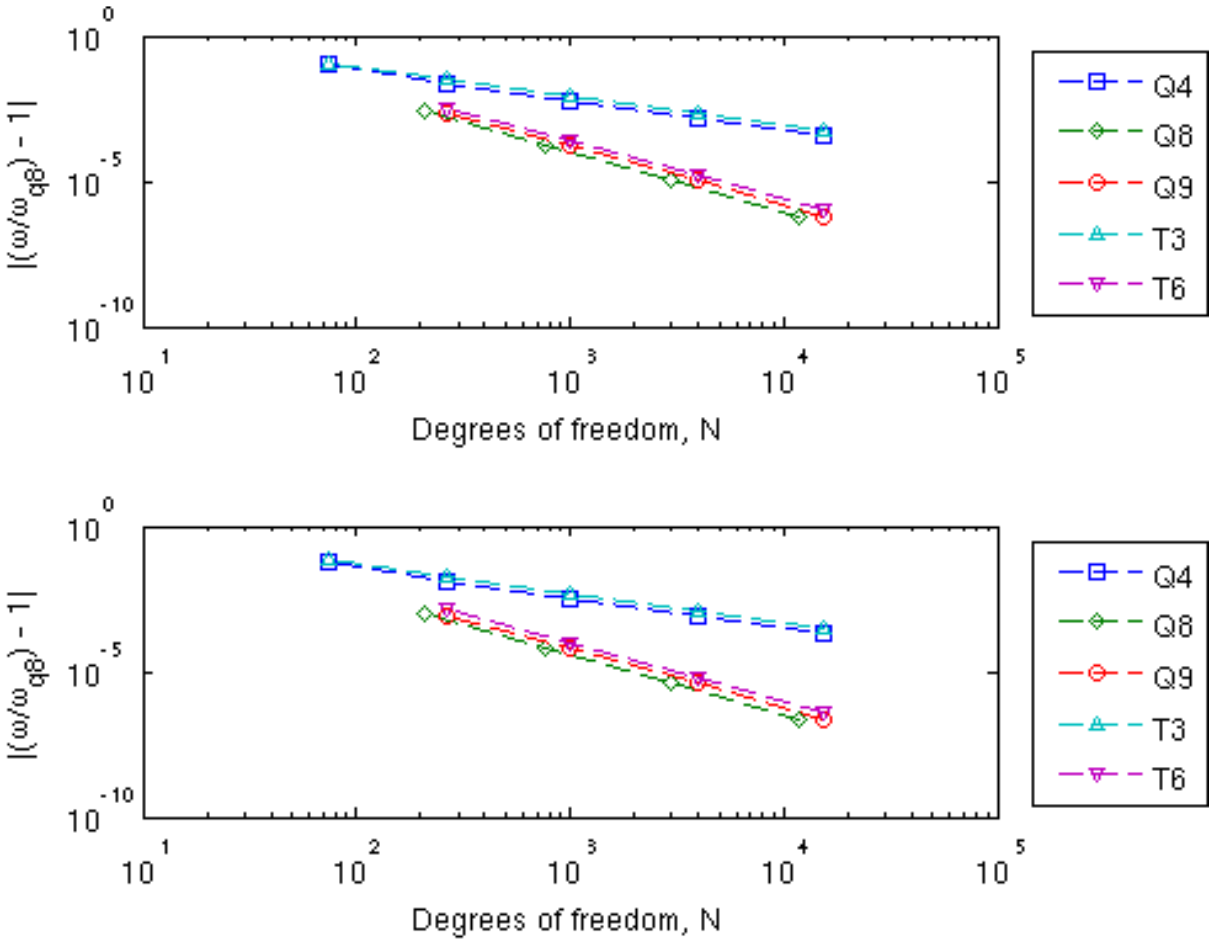

Figure 5: Comparison of convergence rates in the circular cylinder for the various elements

elements, illustrated by the gradients of the dashed lines. It also shows that for a given number of degrees of freedom, the Q8 element is the most accurate element, and in computational terms, seems to be the least expensive. In this case, the convergence rate, $m \approx 1$ for the linear elements and $m \approx 2$ for the quadratic elements.

4.2 Convergence with a Rail Cross-section

The study above was repeated with a rail cross-section instead of a circular cylinder. Figure 6 shows the meshes that were used in the convergence study.

The results obtained for the convergence study are shown in Figure 7. As in the previous study, Figure 7 gives the direct results for two modes whilst Figure 8 shows two modes with the bottom half focussing on the difference between the quadratic elements. Figure 7 and Figure 8 reiterate the results obtained in the previous study. The quadratic elements are seen to be more accurate than the linear elements with the Q8 element proving to be computationally the most economical element as before. The Q8 element was therefore selected to investigate the application of symmetry to model a symmetrical rail profile.

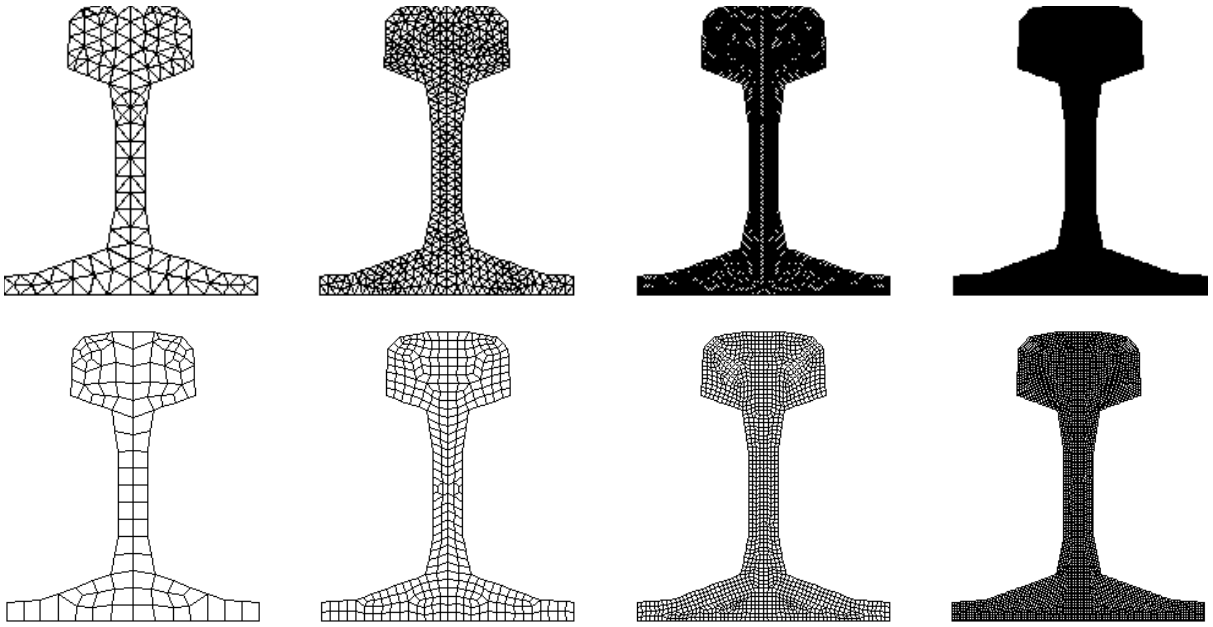

Figure 6: Element meshes of full rail profile — triangular elements (top) and quadrilateral elements (bottom)

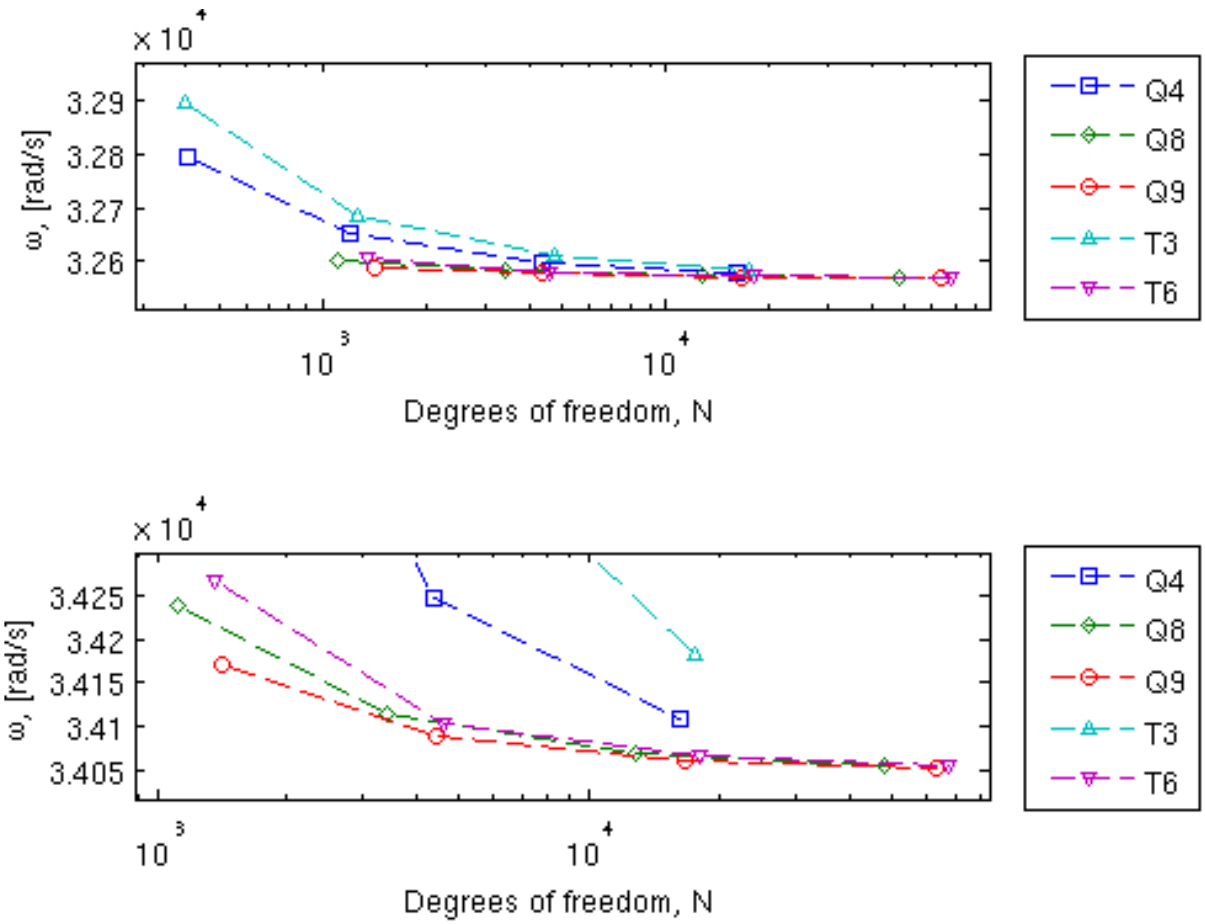

Figure 7: Convergence of two different modes with increasing degrees of freedom in the rail

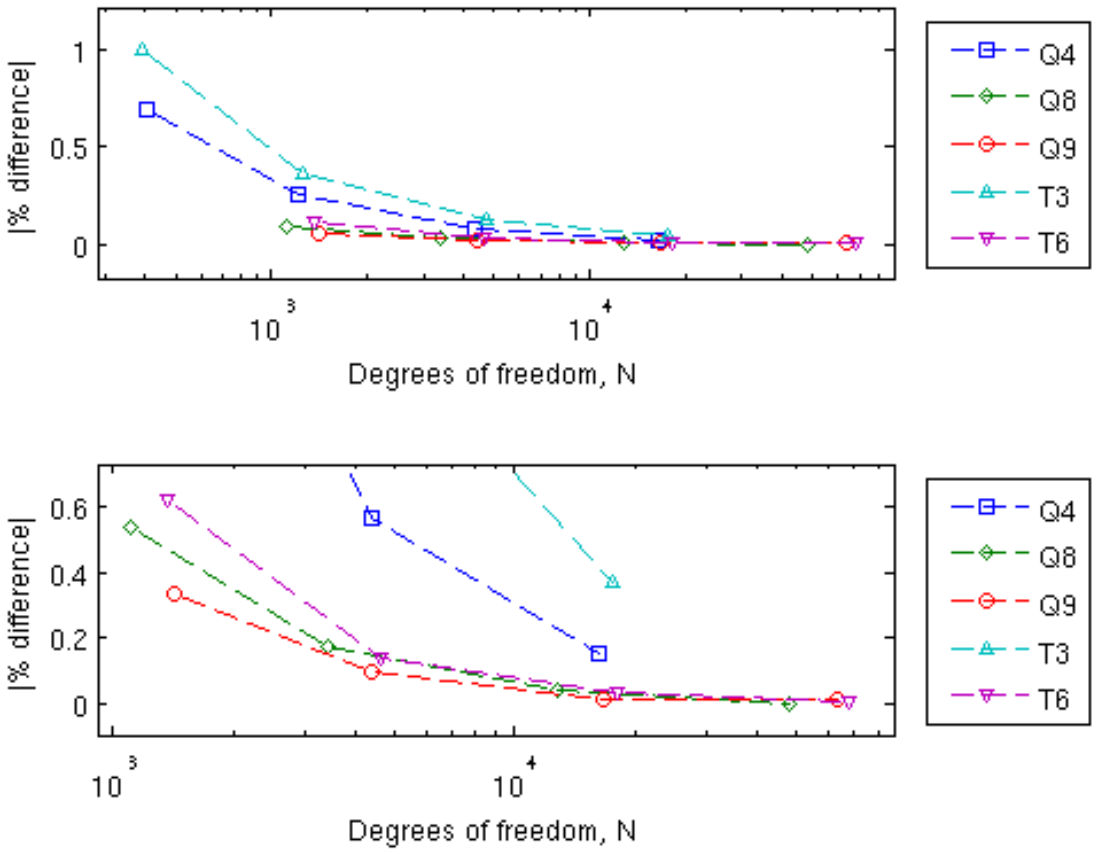

Figure 8: Percentage difference with the best value obtained for the Q8 element

4.3 Investigation of Symmetry Models

The second objective of this paper is to investigate whether a half model with appropriate boundary conditions can replace a full model of a symmetrical waveguide cross-section. The frequencies calculated in each case are compared to check if any vibratory modes were inaccurately predicted by the half model, and if so, what the corresponding modes are.

Based on the results from the convergence study of the rail, the second quadrilateral mesh depicted in Figure 6 (approximately 300 elements) was selected for the study of symmetric and anti-symmetric modes as in [6]. The mesh represents a UIC60 rail profile that is 172mm high and 150mm wide. Instead of the complete cross-section only half the cross-section as shown in Figure 9 was modelled with the appropriate boundary conditions.

In this problem, two sets of boundary conditions apply to capture the modes of the rail. x and y represent the horizontal and vertical directions in the rail's cross-sectional plane while z represents the direction along the length of the rail. For the symmetric modes, the nodes along the left-edge are constrained in the x direction. For the anti-symmetric modes the nodes along the left-edge are constrained in the y and z directions. The full model has no boundary conditions applied to it. Figure 10 illustrates separately the results obtained for each of the models.

Figure 11 shows the dispersion characteristics superimposed, with circles representing the full model and dots representing the half models. Figure 11 shows that for the range of wavenum-

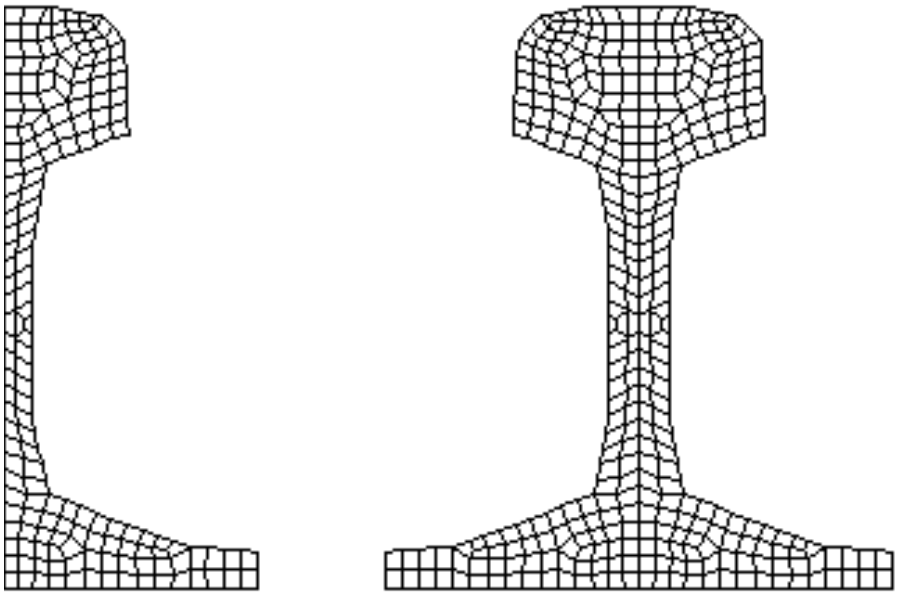

Figure 9: Full and half model of the rail cross-section

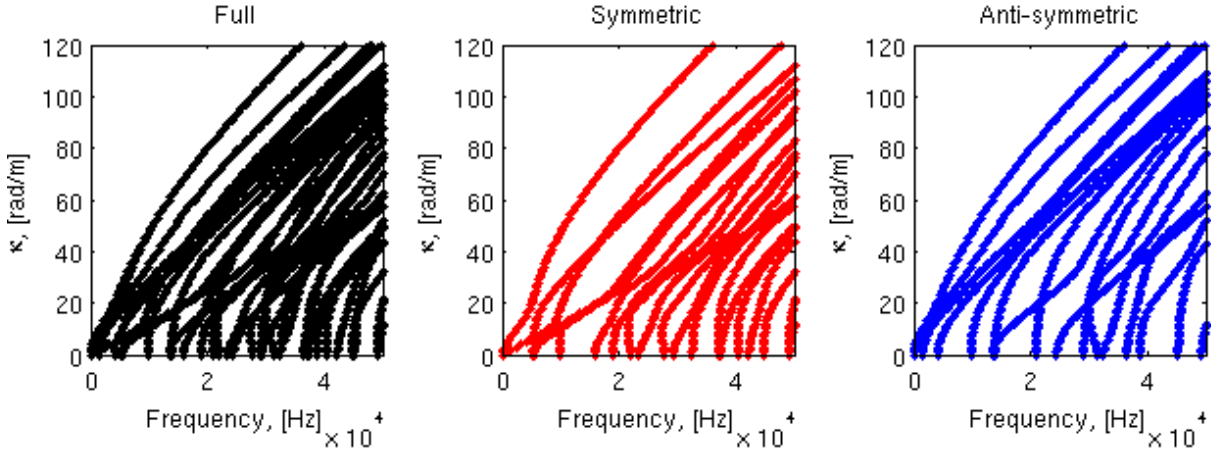

Figure 10: Dispersion characteristics of each model

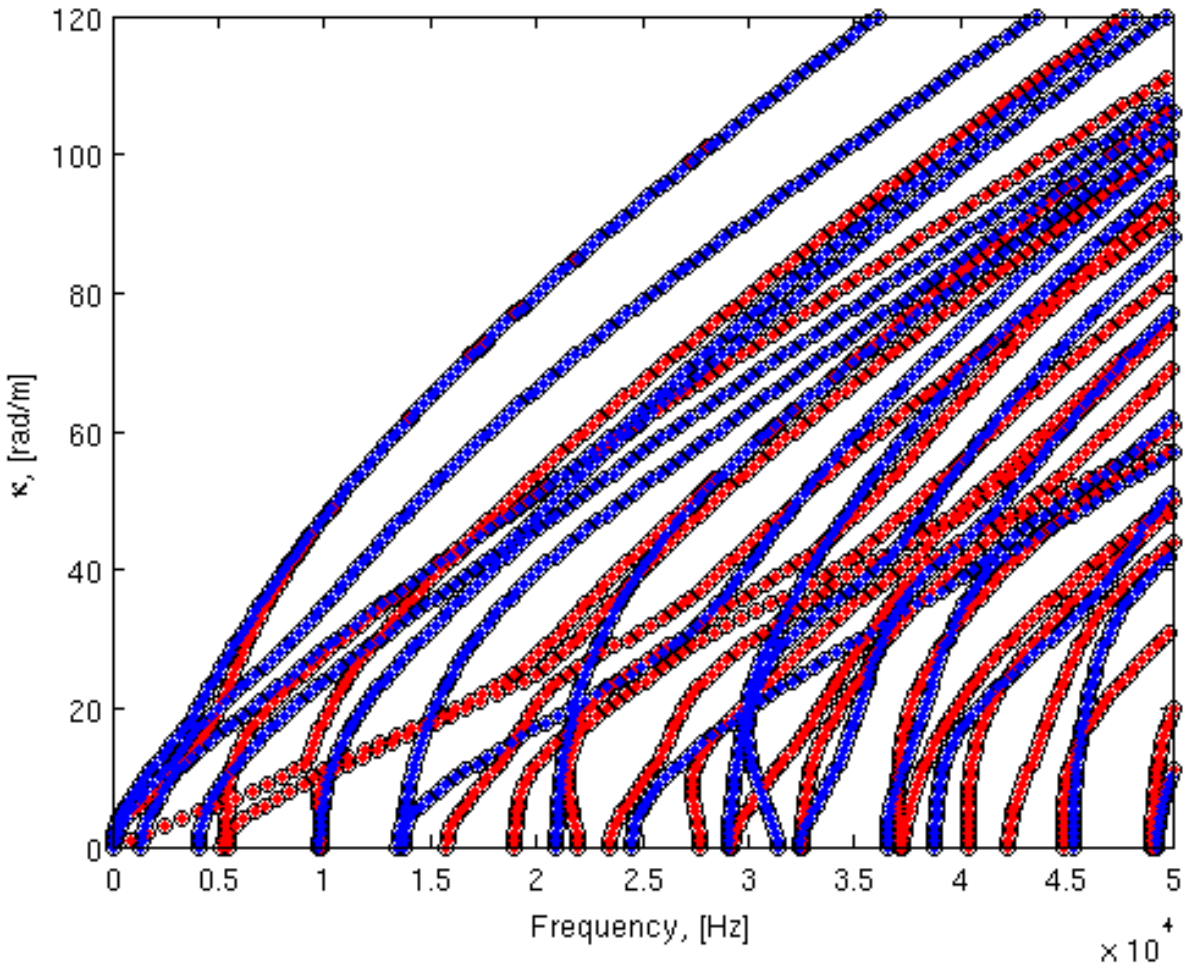

Figure 11: Superimposed dispersion characteristics of the three models

bers investigated, the two half models successfully captured all the modes that are predicted by the full model without exception.

5 Conclusion

The first objective of this paper was to recommend an element for future analysis of rails excited by piezoelectric ultrasonic transducers. Based on the convergence studies presented, the Q8 element is highly recommended for this application owing to its higher accuracy and faster convergence when compared to Q4 or T3 elements for similar number of degrees of freedom. The number of elements recommended to model a rail cross-section is approximately 300 for a maximum error of 0.5%.

The second objective of this paper was to investigate the use of a symmetric half model with appropriate boundary conditions instead of a full model. Based on the results obtained, a half model can indeed be used for this problem as all the modes are captured with the symmetric half model. An obvious requirement of this method is that the rail profile is symmetric.

The paper has therefore suggested two approaches to reduce the amount of computational resources required for a given problem, viz. the use of higher-order elements and, if applicable, the exploitation of geometrical symmetry.

Acknowledgements

The authors would like to sincerely acknowledge the use of MATLAB code originally programmed by Schalk Kok (CSIR) and Nico Wilke (UP). The code was extensively modified to suit the objectives of this paper.

References

[1] L. Gavrić, Computation of propagative waves in free rail using a finite element technique, Journal of Sound and Vibration, 185(3):531-543,c 1995.

[2] V. Damljanović and R.L. Weaver, Propagating and evanescent elastic waves in cylindrical waveguides of arbitrary cross section, J. Acoust. Soc. Am., 115(4):1572-1581, 2004.

[3] T. Hayashi, W.-J. Song, and J. L. Rose, Guided wave dispersion curves for a bar with an arbitrary cross-section, a rod and rail example, Ultrasonics, 41:175183, 2003.

[4] Bartoli, A. Marzani, F. L. di Scalea, and E. Viola, Modelling wave propagation in damped waveguides of arbitrary cross-section, Journal of Sound and Vibration, 295:685707, 2006.

[5] P.W. Loveday, Simulation of Piezoelectric Excitation of Guided Waves using Waveguide Finite Elements, IEEE Trans. Ultrasonics, Ferroelectrics, and Frequency Control, 55(9):2038-2045, 2008.

[6] J. Ryue, D.J. Thompson, P.R. White, D.R. Thompson, Decay rates of propagating waves in railway tracks at high frequencies, Journal of Sound and Vibration, 320:955-976, 2009.

[7] P.W. Loveday, Analysis of Piezoelectric Ultrasonic Transducers Attached to Waveguides Using Waveguide Finite Elements, IEEE Trans. Ultrasonics, Ferroelectrics, and Frequency Control, 54(10):2045-2051, 2007.

[8] T.R. Chandrupatla and A.D. Belegundu, Introduction to Finite Elements in Engineering, 3rd Edition, Prentice Hall, 2002.

[9] A.E. Armenàkas, D.C. Gazis, and G. Herrmann, Free Vibrations of Circular Cylindrical Shells, Pergamon Press, 1969.